The influence of grain size on hydrogen embrittlement of a multicomponent $(FeCrNiMnCo)_{99}N_1$ alloy

Darya Yu. Gurtova[*1], student
Marina Yu. Panchenko[2,3], junior researcher
of Laboratory of Physics of Hierarchic Structures in Metals and Alloys
Evgeny V. Melnikov[2,4], junior researcher
of Laboratory of Physics of Hierarchic Structures in Metals and Alloys
Denis O. Astapov[1,5], student
Elena G. Astafurova[2,6], Doctor of Sciences (Physics and Mathematics),
Head of Laboratory of Physics of Hierarchic Structures in Metals and Alloys

[1]*Tomsk State University, Tomsk (Russia)*
[2]*Institute of Strength Physics and Materials Science of Siberian Branch of RAS, Tomsk (Russia)*

*E-mail: dasha_gurtova@mail.ru

[3]ORCID: https://orcid.org/0000-0003-0236-2227
[4]ORCID: https://orcid.org/0000-0001-8238-6055
[5]ORCID: https://orcid.org/0000-0002-1277-4180
[6]ORCID: https://orcid.org/0000-0002-1995-4205

Abstract: The problem of hydrogen embrittlement remains relevant in many areas, so the FeCrNiMnCo alloy (Cantor alloy) generates increased interest among researchers as one of the materials least exposed to the negative effect of hydrogen. Nevertheless, the issue of the influence of microstructure parameters on hydrogen embrittlement of the Cantor alloy and multicomponent alloys of the FeCrNiMnCo system in general remains understudied. This work studies the influence of grain size on the susceptibility of a nitrogen-doped high-entropy Cantor alloy to hydrogen embrittlement. For this purpose, states with different grain sizes (43±21, 120±57, and 221±97 μm) were formed in the $(FeCrNiMnCo)_{99}N_1$ alloy, using thermomechanical treatments. It is experimentally found that grain refinement leads to an increase in the strength properties of the alloy under study and promotes an increase in the resistance to the hydrogen embrittlement: in samples with the smallest grain size, the hydrogen-induced decrease in ductility is less than in samples with the largest one. A decrease in grain size causes as well a decrease in the length of the brittle zone detected on the fracture surfaces of samples after tension. This is caused by a decrease in hydrogen diffusion during the hydrogen-charging process and a decrease in the transport of hydrogen atoms with mobile dislocations during plastic deformation due to a decrease in grain size.

Keywords: hydrogen embrittlement; multicomponent alloys; high-entropy alloys; Cantor alloy; $(FeCrNiMnCo)_{99}N_1$; hydrogen-induced brittle zone; grain boundaries; fracture; mechanical properties.

For citation: Gurtova D.Yu., Panchenko M.Yu., Melnikov E.V., Astapov D.O., Astafurova E.G. The influence of grain size on hydrogen embrittlement of a multicomponent $(FeCrNiMnCo)_{99}N_1$ alloy. *Frontier Materials & Technologies*, 2024, no. 3, pp. 41–51. DOI: 10.18323/2782-4039-2024-3-69-4.

INTRODUCTION

It is known that hydrogen has a negative effect on metals and alloys, leading to a deterioration in their properties and a reduction in service life. The issue of the need to create new structural materials resistant to the negative effects of hydrogen, and to find methods for reducing the tendency to hydrogen embrittlement for existing materials is acute today in many industries, including nuclear energy, the oil and gas industry, and promising and rapidly developing hydrogen energy indus-

try. Currently, structural elements used in hydrogen-containing working environments are made of stable austenitic steels as well-proven materials, that are least prone to hydrogen embrittlement among steels of various classes. However, the high-entropy FeCrNiMnCo alloy named after its discoverer B. Cantor demonstrates greater resistance to the hydrogen embrittlement effects than the above-mentioned austenitic steels under the same hydrogen-charging conditions [1; 2]. Besides, Cantor alloy has unique mechanical and physical

properties: resistance to radiation damage and corrosion, wear resistance, a combination of high ductility and strength, due to which it can be used even in extreme conditions [3; 4]. However, the alloy has a relatively low yield strength [5]. One of the most effective methods to solve this problem is considered to be doping the alloy with interstitial atoms, in particular nitrogen, to increase the strength properties of the material without significant loss of ductility [6; 7].

In addition, it has been found that alloying materials also affects their susceptibility to hydrogen embrittlement. Thus, in [8] it was found that alloying the CoCrFeNi alloy with aluminum helps to increase resistance to the hydrogen embrittlement effects, as well as an increase in strength and ductility. In the work [9], covering the study of the hydrogen embrittlement in the Cantor alloy, it is shown that adding of 0.5 at. % carbon increases the alloy susceptibility to the hydrogen negative effects. At the same time, works [10; 11] found that alloying with carbon, on the contrary, can increase the resistance of the Cantor alloy and alloys based on it to hydrogen-induced degradation of mechanical characteristics. The ambiguity of the results obtained, when studying the influence of interstitial atoms on hydrogen embrittlement of the Cantor alloy, necessitates further development of this scientific problem.

It is known that the diffusion of hydrogen is a critical parameter affecting the hydrogen embrittlement of alloys [12]. A significant aspect affecting the hydrogen diffusion is the sites of its capture (so-called traps), which usually include interstices, dislocations, grain boundaries and interphase boundaries, cracks, particles, etc. [13–15]. Increasing the number of traps, for example, grain boundaries, by grain refinement makes it possible to reduce the hydrogen negative impact on metals and alloys. In works [16; 17], it was found that reducing the grain size in the Cantor alloy reduces the specific concentration of hydrogen at the grain boundaries, while suppressing brittle cracking and increasing the alloy's resistance to hydrogen embrittlement. Based on this, studying the influence of grain size on hydrogen embrittlement in a multicomponent Cantor alloy doped with nitrogen atoms is of interest.

The purpose of this study is to identify the patterns of hydrogen embrittlement of the $(FeCrNiMnCo)_{99}N_1$ high-entropy alloy with different grain sizes.

METHODS

A multicomponent high-entropy alloy based on Cantor alloy (HEA-N) was chosen as the object of study. Cast billets were obtained by induction melting of Cr, Ni, Fe, Co powders with the manganese nitride addition. The composition specified during melting corresponded to the stoichiometric ratio of $(FeCrNiMnCo)_{99}N_1$ (19.8Fe–19.8Cr–19.8Ni–19.8Mn–19.8Co–1N, at. %).

The cast billets were subjected to heat treatment, which consisted of annealing at a temperature of 1200 °C for 2 h followed by quenching in water. After this, the billets were rolled to 80 % reduction. To obtain states with different grain sizes, the rolled bars were soaked at different temperatures, and quenched in water:

to obtain the smallest grain size (S_HEA-N) – at a temperature of 1000 °C for 1 h; medium (M_HEA-N) – at a temperature of 1100 °C for 1 h; coarse grains (C_HEA-N) – at a temperature of 1200 °C for 2 h. After all thermomechanical treatments, the samples had the chemical composition: 19.9Fe–20.1Cr–20.0Ni–19.9Mn–19.3Co–0.8N, at. %. The elemental composition of the samples (Co, Cr, Ni, Mn, and Fe) was analyzed using a LEO EVO 50 scanning electron microscope (Zeiss, Germany), with a device for energy-dispersive spectroscopy. Nitrogen concentration was determined using a LECO ONH spectrometer (LECO, USA).

Dumbbell-shaped tensile samples of $12 \times 2.6 \times 1.4$ mm³ in gauge section, were cut from the resulting blanks on an electric spark machine.

Electrochemical hydrogen-charging of the samples was carried out at room temperature in a 3 % aqueous NaCl solution containing 3 g/L of NH_4SCN as a recombination poison. The charging duration was 50 h at a current density of 10 mA/cm².

The intensity of hydrogen desorption from the surface of the samples was analyzed by thermal desorption spectroscopy (TDS). The samples were studied in the temperature range of 25–800 °C (heating rate is 4 °C/min), using a vacuum chamber with the simultaneous collection of thermal desorption spectra by an RGA100 quadrupole mass spectrometer (Stanford Research Systems, USA). The hydrogen concentration profile over the depth of the samples was obtained using a GD-Profiler 2 glow discharge optical emission spectrometer (Horiba, France).

The microstructure of the samples was studied using an Apreo 2 S scanning electron microscope (FEG SEM), equipped with a Velocity Super system for analyzing the structure and texture of crystalline materials, by the electron backscattered diffraction (EBSD) method. The average grain size was determined by the interseption method using electron microscopic photographs (without taking into account twin boundaries).

Uniaxial tension tests of the samples were carried out with the initial strain rates of 5×10^{-4} s⁻¹ and 1×10^{-2} s⁻¹ on an electromechanical machine LFM-125 (Walter+Bai AG, Switzerland), at room temperature. Mechanical tests were also carried out at a strain rate of 1×10^{-2} s⁻¹ at low temperature (−196 °C) on an electromechanical machine Instron 1185 (Instron, USA). At least 5 samples were used to validate each condition.

RESULTS

After thermomechanical treatments according to the selected modes, three types of samples with different grain sizes were formed. All states have a single-phase (γ-fcc) structure. According to the images obtained by the EBSD method, all the studied samples are characterized by a disordered polycrystalline structure; no predominant grain orientation is observed. Moreover, the structure contains a large number of annealing twins, which may indicate a rather low energy of stacking faults in the alloy under study (Fig. 1). The average grain size of all samples received is presented in Table 1.

For all the studied samples, the TDS curves (Fig. 2) show one low-temperature peak with a maximum intensity at about 145 °C, which characterizes the desorption of diffusible hydrogen trapped in the crystal lattice or weak reversible traps: interstices, dislocations, vacancies, grain boundaries. In this case, changes in grain size have little effect on the position and intensity of the TDS peak.

According to the stress–strain diagrams (Fig. 3), grain refinement leads to an increase in the yield strength and ultimate tensile strength of the HEA-N alloy, and a slight decrease in its ductility.

The influence of hydrogen-charging of samples with different grain sizes on their mechanical characteristics, such as yield strength $\sigma_{0.2}$, ultimate tensile strength σ_{UTS}, elongation to failure δ, and hydrogen embrittlement index I_H is shown in Table 2. The I_H value characterizing the reduction in ductility caused by hydrogen, was defined as

$$I_H = \frac{\delta_0 - \delta_H}{\delta_0} \times 100\%,$$

where δ_0 and δ_H are the total elongation to failure of the samples before and after hydrogen-charging, respectively.

Electrochemical hydrogen-charging does not contribute to the occurrence of noticeable effects of solid solution strengthening by hydrogen atoms, consequently, without causing a significant change in the value of the yield strength $\sigma_{0.2}$. Hydrogen-charging leads as well to a decrease in tensile strength σ_{UTS}, and the smallest decrease is observed in S_HEA-N samples with a minimum grain size.

The hydrogen embrittlement index I_H has a maximum value in C_HEA-N samples with the largest grain size, and a significant decrease in the I_H value is observed with decreasing grain size. In S_HEA-N samples with the smallest grain size ($d=43\pm21$ μm), the value of $I_H \approx 0$: a hydrogen-induced decrease in plasticity under these charging conditions, is not observed in such samples. Thus, grain structure refinement helps to increase the resistance of the studied HEA-N alloy to the hydrogen embrittlement effects.

Hydrogen-charging of samples leads to the formation of a brittle surface layer, which undergoes intense cracking during deformation (Fig. 4). The fracture behavior of the side surfaces of hydrogen-charged samples is predominantly intergranular, but single transgranular cracks are also observed in M_HEA-N and C_HEA-N samples (Fig. 4 a–c). Despite the brittle fracture behavior, a large number of slip lines are observed on the side surfaces.
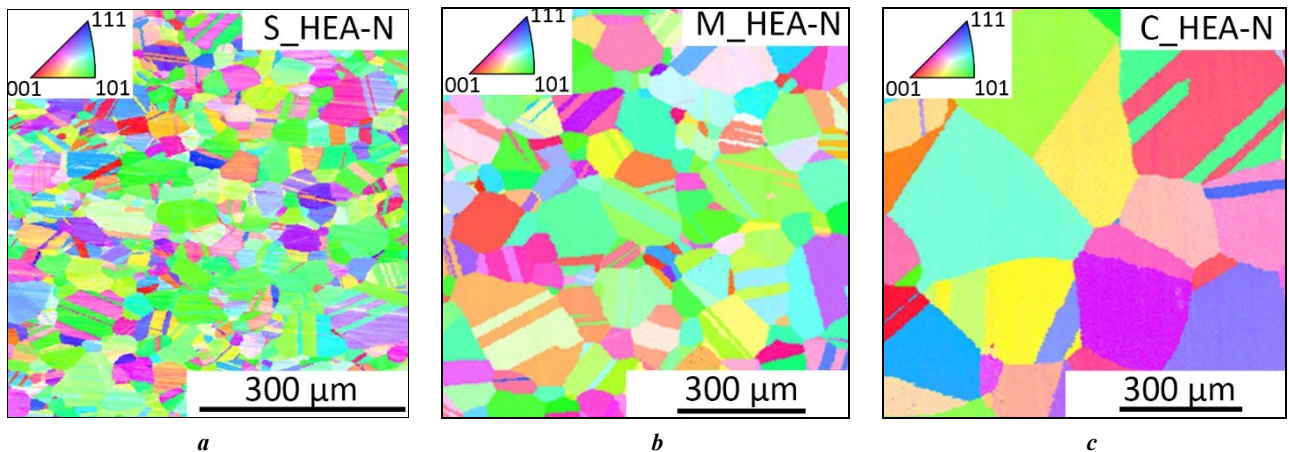
Fig. 1. *EBSD image of the microstructure of samples:* **a** *– with the smallest grain size (S_HEA-N);*
b *– with the medium grain size (M_HEA-N);* **c** *– with the largest grain size (C_HEA-N)*
Рис. 1. *ДОЭ-изображения микроструктуры образцов:* **a** *– с меньшим размером зерна (S_HEA-N);*
b *– со средним размером зерна (M_HEA-N);* **c** *– с самым крупным размером зерна (C_HEA-N)*

Table 1. *The average size of austenitic grains in the alloy under study depending on the treatment mode*
Таблица 1. *Средний размер аустенитных зерен в исследуемом сплаве в зависимости от режима обработки*

HEA-N	Treatment mode		
	1000 °C, 1 h	1100 °C, 1 h	1200 °C, 2 h
Average grain size d, μm	43±21	120±57	221±97
Designation	S_HEA-N	M_HEA-N	C_HEA-N
Phase composition	γ-phase		
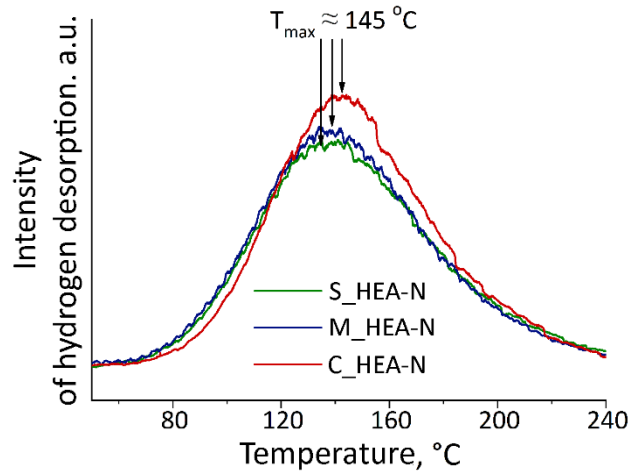
Fig. 2. *TDS spectra of hydrogen desorption for the (FeCrMnCoNi)$_{99}$N$_1$ alloy samples with different grain sizes*
Рис. 2. *ТДС-спектры десорбции водорода для образцов сплава (FeCrMnCoNi)$_{99}$N$_1$ с разным размером зерна*
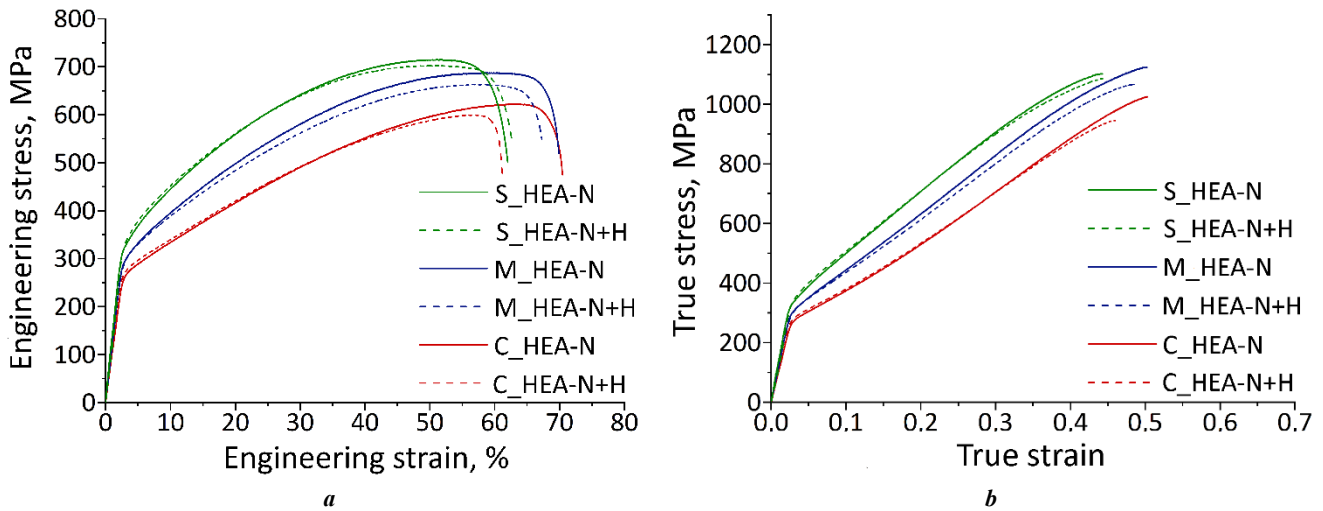
Fig. 3. *Strain-stress diagrams of the samples with the smallest (S_HEA-N), medium (M_HEA-N)*
and the largest (C_HEA-N) grain size before and after hydrogen-charging (+H):
a *– engineering coordinates;* ***b*** *– true coordinates*
Рис. 3. *Диаграммы растяжения образцов с малым (S_HEA-N), средним (M_HEA-N)*
и крупным (C_HEA-N) размером зерна до и после наводороживания (+H):
a *– инженерные координаты;* ***b*** *– истинные координаты*

Table 2. *The influence of hydrogen-charging (+H) on the mechanical properties of a HEA-N alloy with different grain sizes*
Таблица 2. *Влияние насыщения водородом (+H) на механические свойства сплава ВЭС-N с разным размером зерна*

Material	$\sigma_{0.2}$, MPa (±5 MPa)	σ_{UTS}, MPa (±10 MPa)	δ, % (±2 %)	I_H, %
S_HEA-N	310	715	58	0
S_HEA-N+H	312	703	58	
M HEA-N	282	688	65	6
M_HEA-N+H	285	663	61	
C_HEA-N	252	622	66	14
C HEA-N+H	260	600	57	

According to SEM analysis of the fracture surfaces, the central part of the samples after hydrogen-charging fractures in a ductile transgranular regime with the formation of a dimple fracture (Fig. 4 d–f). The fracture mechanism and the length of the brittle zone in the fracture depend on the grain size of hydrogen-charged samples. The fracture behavior of the brittle zone in coarse-grained C_HEA-N samples is mixed – both transgranular and intergranular facets are observed. Reducing the grain size helps to reduce the proportion of transgranular cracks in the M_HEA-N samples and almost completely suppresses the transgranular fracture in the S_HEA-N samples.

The length of the hydrogen-induced brittle zone D after mechanical tensile tests at room temperature, does not correspond to the initial thickness of the hydrogen-assisted layer, formed immediately after electrochemical hydrogen-charging (D_0), since during plastic deformation hydrogen atoms are redistributed on mobile dislocations (ΔD_d) and due to diffusion under stress (ΔD_s).

The brittle zone in the fracture of hydrogen-charged samples is characterized by the greatest length in all samples subjected to deformation in mode I. Changing the tensile mode for all samples leads to a reduction in the brittle zone length to a minimum (mode III), due to the suppression of hydrogen transport during deformation (Table 3). The same patterns can be observed for all modes of mechanical tests: the maximum length of the hydrogen-induced brittle zone is characteristic of coarse-grained C_HEA-N samples, and grain refinement leads to its reduction (Table 3).

Fig. 5 shows the hydrogen distribution profile in the structure of coarse-grained C_HEA-N samples. Comparison of data in Fig. 5 with the results given in Table 3, showed that in the case when the diffusion and dislocation transport of hydrogen is suppressed (mode III), the brittle zone length has values close to the thickness of the hydrogen-induced surface layer.

DISCUSSION

The results of the analysis of thermal desorption curves of the high-entropy alloy under study differ from those obtained in works studying hydrogen embrittlement in traditional materials with one basic component. For the cases of
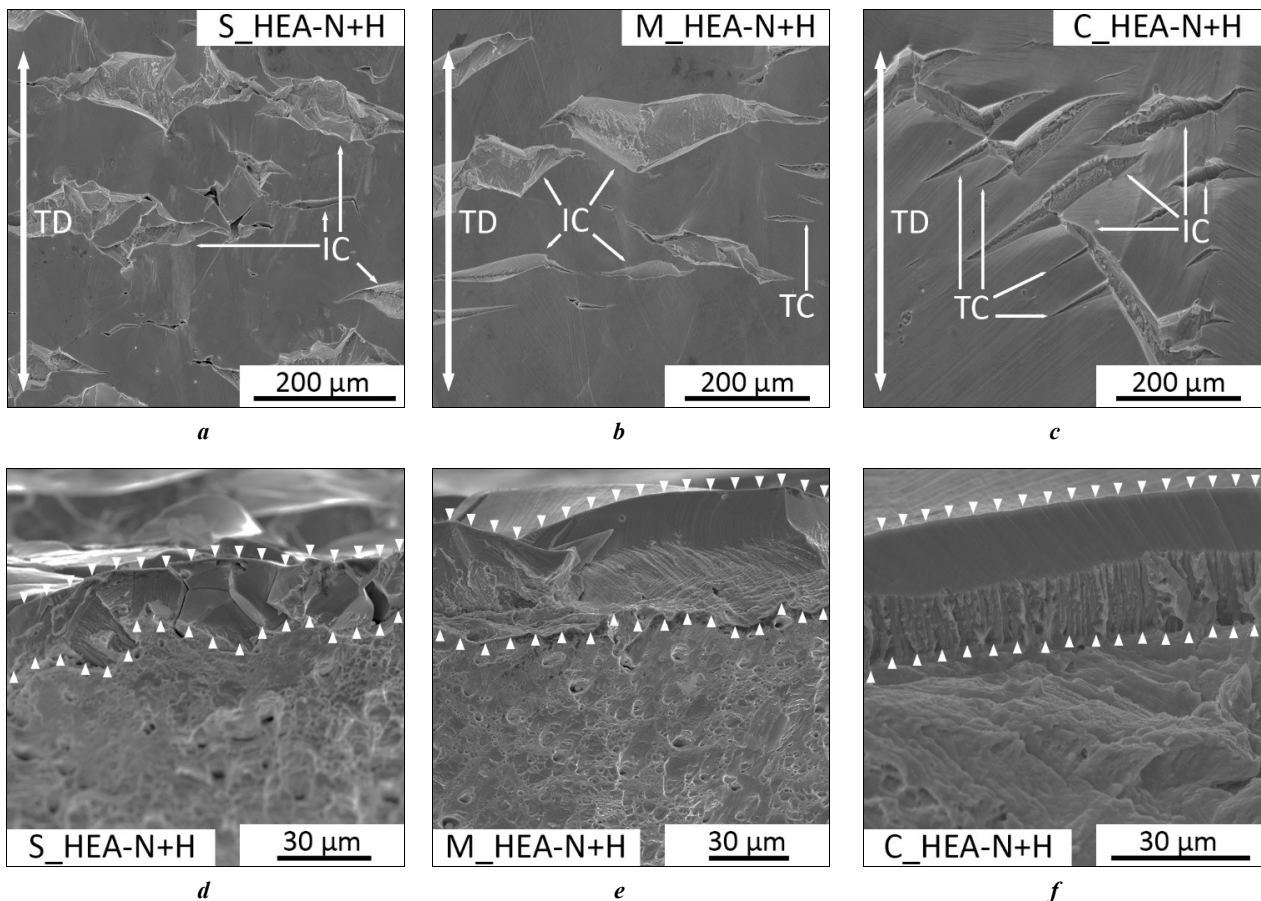
*Fig. 4. SEM images of hydrogen-charged (+H) samples with the smallest (S_HEA-N), medium (M_HEA-N)
and the largest (C_HEA-N) grain size after failure:
a, b, c – side surface; d, e, f – fracture surface
(TD – tension direction, IC – intergranular cracks, TC – transgranular cracks)*
*Рис. 4. СЭМ-изображения насыщенных водородом (+H) образцов с малым (S_HEA-N), средним (M_HEA-N)
и крупным (C_HEA-N) размером зерна после растяжения:
a, b, c – боковая поверхность; d, e, f – поверхность разрушения
(TD – направление растяжения, IC – интеркристаллитные трещины, TC – транскристаллитные трещины)*

Table 3. *Modes of mechanical tensile tests of hydrogen-charged samples of the HEA-N alloy with the smallest (S_HEA-N), medium (M_HEA-N) and the largest (C_HEA-N) grain size and their influence on the length of a brittle zone in a fracture*
Таблица 3. *Режимы механических испытаний на растяжение насыщенных водородом образцов сплава ВЭС-N с малым (S_HEA-N), средним (M_HEA-N) и крупным (C_HEA-N) размером зерна и их влияние на длину хрупкой зоны в изломе*

Deformation parameters and characteristics of brittle zone		Mode		
		I	II	III
Strain rate, c^{-1}		5×10^{-4}	1×10^{-2}	1×10^{-2}
Testing temperature, K		293	293	77
Hydrogen transport on dislocations		active	significantly suppressed	suppressed
Hydrogen transport due to the stress-assisted diffusion		active	active	suppressed
Brittle zone length *D*, μm	S_HEA-N	25±5	20±6	12±3
	M_HEA-N	33±7	25±8	13±5
	C_HEA-N	35±12	27±8	18±7

austenitic [18], ferritic [19] and martensitic [20] steels, it has been shown that a decrease in grain size leads to an increase in the content of diffusible hydrogen in the samples (in the crystal lattice or weak reversible traps). In this case, the hydrogen-charging modes of all the above materials were the same.

In [18], the smallest grain size presented was 0.58 μm, the maximum was 19 μm, while the hydrogen concentration in coarse-grained samples was 3.3 wppm (weight parts per million), which is more than two times less than in ultrafine-grained samples (7.1 wppm). For the HEA-N alloy, the decrease in grain size by ≈2 times for M_HEA-N samples (*d*=120±57 μm) and by ≈5 times for S_HEA-N samples (*d*=43±21 μm) relative to samples with the largest grain size C_HEA-N (*d*=221±97 μm) does not lead to significant differences in the thermal desorption curves: the intensity and position of the TDS peaks do not undergo significant changes. This is consistent with the data of [16],

where similar results were obtained for the equiatomic high-entropy Cantor alloy without interstitial atoms and with grain sizes from 1.5 to 22 μm, which was saturated with hydrogen from a gas atmosphere. In [16], the author concludes that in steels of different classes, grain boundaries play a significant role in the hydrogen trapping, while in the multicomponent Cantor alloy, hydrogen atoms are trapped mainly by the crystal lattice interstices.

A noticeable increase in resistance to the hydrogen embrittlement effects expressed in a decrease in the values of the hydrogen embrittlement index I_H, is observed in HEA-N samples with a small grain size. Typically, a decrease in the susceptibility to hydrogen embrittlement during grain refinement is associated with the fact that when a large number of grain boundaries are formed, the amount of absorbed hydrogen in the grains [1] and its content per unit of boundary area decreases, which reduces the stress concentration at the grain boundaries.
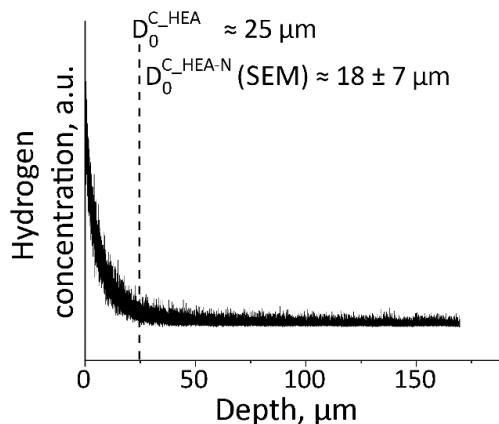
Fig. 5. *Hydrogen concentration profile for the samples with the largest grain size (C_HEA-N)*
Рис. 5. *Концентрационный профиль водорода для образцов с крупным размером зерна (C_HEA-N)*

By analyzing the data obtained experimentally, as a result of mechanical tests for uniaxial tension in various modes (Table 3), the length of the brittle zone in the fracture immediately after hydrogen-charging was assessed, as well as the contributions to the hydrogen transfer by dislocation transport and due to diffusion under stress during the deformation process. However, numerous factors influencing the brittle zone formation in the process of plastic deformation do not allow obtaining exact quantitative values for each of the contributions; therefore, this assessment method makes it possible only to qualitatively establish the patterns of the grain size influence on the hydrogen behavior in the material.

As stated earlier, the suppression of both contributions to hydrogen redistribution at cryogenic test temperatures and high strain rates makes the length of the hydrogen-induced brittle zone formed after mode III (D_{III}) of deformation closest to the length of the brittle zone immediately after electrochemical charging (without deformation) D_0.

The length of the brittle zone in samples deformed in mode II significantly exceeds the values characteristic of samples deformed in mode III (Table 3). For low degrees of plastic deformation, when the dislocation range is limited primarily by grain boundaries and dislocation transport of hydrogen can be realized over long distances, dislocation densities of the order of 10^{12} 1/m^2 are typical. With such a dislocation density and strain rate of $SR=10^{-2}$ 1/s, the rate of dislocation movement is $v=4\times10^{-5}$ m/s ($SR=\rho bv$, $b=2.55$ Å – dislocation Burgers vector). In that case, the time during which a dislocation moves one interatomic distance $a=3.6$ Å is $\tau=9\times10^{-6}$ s, and the movement of hydrogen on the cores of mobile dislocations requires that the diffusion coefficient be $D=7\times10^{-15}$ m^2/s ($D=a^2/2\tau$ [21]). This value is significantly greater than that characteristic of hydrogen diffusion in the crystal lattice of gamma iron at room temperature ($D=1\times10^{-16}$ m^2/s [22]). Thus, at a strain rate of $SR=10^{-2}$ 1/s (mode II) dislocation transport is significantly suppressed, and the brittle zone length increases relative to the values characteristic of deformation in mode III mainly due to hydrogen lattice diffusion under stress (ΔD_s).

Assuming that the length of the brittle zone in the fracture of hydrogen-charged samples subjected to deformation mode I is determined by the additive contributions of different hydrogen transfer mechanisms ($D_I\approx D_0+\Delta D_d+\Delta D_s$), one can find the joint contribution from transport on dislocations (ΔD_d) and from stresses (ΔD_s) as follows $D_I-D_{III}=\Delta D_d+\Delta D_s$. The contribution of hydrogen transfer by diffusion under stress can be roughly estimated as $\Delta D_s=D_I-D_{II}$. Further, it is possible to estimate to a first approximation the contribution of dislocation transport ΔD_d to the brittle zone length. Fig. 6 presents the results of estimates of the D_0, ΔD_d and ΔD_s contributions to the length of the hydrogen-induced brittle zone in the alloy under study, depending on the grain size.

The greatest length of the brittle zone immediately after hydrogen-charging D_0 is observed in coarse-grained C_HEA-N samples. The D_0 value decreases with decreasing grain size (Fig. 6). Since the D_0 value is determined solely by the hydrogen distribution during charging, it depends only on the diffusion of hydrogen atoms in the material during hydrogen-charging. The effective hydrogen diffusion coefficient in samples can be estimated using the formula [21]

$$x \approx \sqrt{2D_{eff}t}, \qquad (1)$$

where x is the characteristic diffusion path;
D_{eff} is an effective diffusion coefficient;
t is the hydrogen-charging duration.

The D_0 length can be taken as the characteristic diffusion path x, since analysis of the profile of hydrogen concentration distribution along the depth of coarse-grained C_HEA-N samples shows the consistency of the results between the experimentally obtained hydrogen distribution along the depth immediately after charging and the length of the brittle zone in the fracture $D_{III}\approx D_0$ estimated by SEM-images of the fracture surface of C_HEA-N samples (Fig. 5, 6).

An assessment of the effective diffusion coefficient (1) of hydrogen in samples of the studied HEA-N alloy shows that a decrease in grain size contributes to a decrease in D_{eff}:
$D_{eff}^{C\_HEA-N} \approx 9\times10^{-16}$ m^2/s, $D_{eff}^{M\_HEA-N} \approx 5\times10^{-16}$ m^2/s and $D_{eff}^{S\_HEA-N} \approx 4\times10^{-16}$ m^2/s. The obtained D_{eff} values are of the same order; however, the minimum value is characteristic of samples with the smallest grain size. Thus, a decrease in grain size or, in other words, an increase in the density of grain boundaries (including an increase in the number of annealing twins) leads to the suppression of hydrogen diffusion deep into the samples. Despite the existence of dual opinions about the influence of grain boundaries and twins on the hydrogen behavior in the material [21; 23; 24], they can act both as traps for hydrogen atoms and as preferential paths for their diffusion. In this work, in samples of the HEA-N alloy within the given conditions of hydrogen charging, they rather play the role of capture sites, although the second option should not be completely excluded.

The grain size of the studied HEA-N samples affects both the hydrogen distribution during charging, and the hydrogen diffusion, during plastic deformation (Fig. 6). Changes in the grain size of the studied samples have a weak effect on the hydrogen diffusion under stress during plastic deformation (Fig. 6). At the same time, the hydrogen transfer by mobile dislocations, directly depends on the grain size. The contribution of dislocation transport decreases with decreasing grain size and reaches a minimum value in the S_HEA-N samples. They are two times smaller than in the coarse-crystalline C_HEA-N samples, which is associated with a decrease in the free path of dislocations during plastic deformation.

CONCLUSIONS

Using various types of thermomechanical treatment, a series of states with different grain sizes was formed in the (FeCrNiMnCo)$_{99}$N$_1$ alloy: 43±21 (S_HEA-N), 120±57 (M_HEA-N), and 221±97 μm (C_HEA-N).

Grain refinement helps to increase the strength properties of the alloy under study and reduce the elongation to
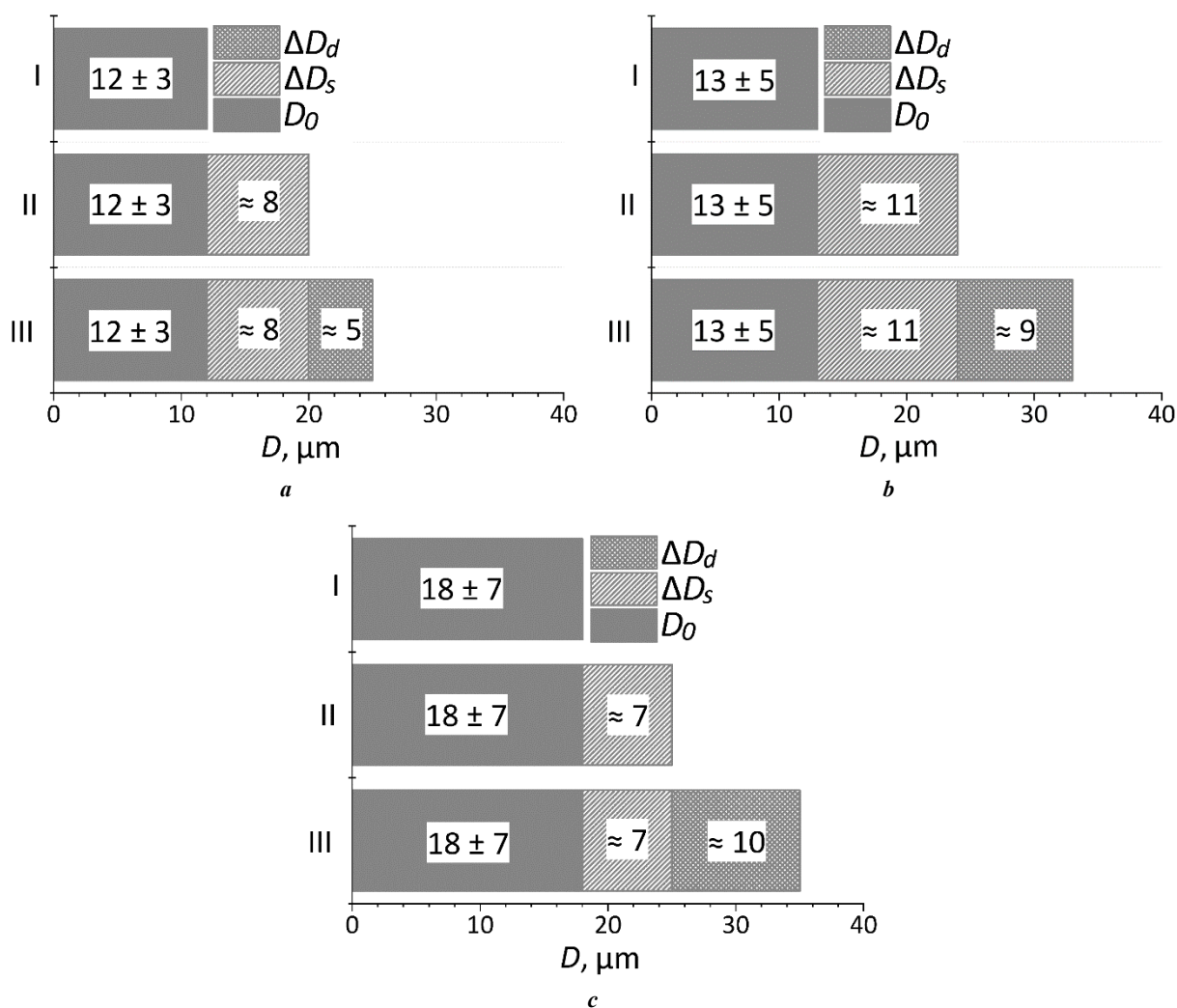
Fig. 6. *The influence of a mechanical testing mode on the length of a brittle hydrogen-induced zone and evaluation of the main contributions from diffusion and dislocation hydrogen transport during plastic deformation of samples with the smallest (S_HEA-N) (**a**), medium (M_HEA-N) (**b**), and the largest (C_HEA-N) (**c**) grain size*

Рис. 6. *Влияние режима механических испытаний на длину хрупкой водородно-индуцируемой зоны и оценка основных вкладов от диффузионного и дислокационного транспорта водорода при пластической деформации образцов с малым (S_HEA-N) (**a**), средним (M_HEA-N) (**b**) и крупным (C_HEA-N) (**c**) размером зерна*

failure, the values of which in all cases remain high (δ_{S_HEA-N}=58 %, δ_{M_HEA-N}=65 %, δ_{C_HEA-N}=66 %).

Hydrogen charging of samples of the alloy under study has little effect on the yield strength, however, leads to a decrease in the ultimate tensile strength and elongation to failure. The formed hydrogen-induced surface zone in samples with the largest grain size, is fractured in a brittle way; cracks are observed both along the body of the grains, and along their boundaries on the side surfaces of the destroyed hydrogen-charged samples. An increase in the number of grain boundaries due to grain refinement is accompanied by a change in the nature of the fracture of the surface brittle hydrogen-assisted zone to a predominantly intergranular one.

It has been experimentally found that a decrease in grain size helps to increase the resistance of the $(FeCrNiMnCo)_{99}N_1$ alloy to the negative effects of hydrogen. This is manifested by a decrease in the hydrogen embrittlement index, as well as in a decrease in the length of the hydrogen-induced brittle zone detected on the fracture surfaces. This is caused by a decrease in the effective coefficient of hydrogen diffusion in the material, as well as a decrease in the free path of dislocations transferring hydrogen deep into the material during plastic deformation.

REFERENCES

1. Feng Zheng, Li Xinfeng, Song Xiaolong, Gu Tang, Zhang Yong. Hydrogen Embrittlement of CoCrFeMnNi High-Entropy Alloy Compared with 304 and IN718 Alloys. *Metals*, 2022, vol. 12, no. 6, article number 998. DOI: 10.3390/met12060998.

2. Zhao Yakai, Lee Dong-Hyun, Seok Moo-Young, Lee Jung-A, Phaniraj M.P., Suh Jin-Yoo, Ha Heon-Young, Kim Ju-Young, Ramamurty U., Jang Jae-il. Resistance of CoCrFeMnNi high-entropy alloy to gaseous hydrogen embrittlement. *Scripta Materialia*, 2017, vol. 135, pp. 54–58. DOI: 10.1016/j.scriptamat.2017.03.029.

3. Cantor B., Chang I.T.H., Knight P., Vincent A.J.B. Microstructural development in equiatomic multi-component alloys. *Materials Science and Engineering: A*, 2004, vol. 375-377, pp. 213–218. DOI: 10.1016/j.msea.2003.10.257.

4. Cantor B. Multicomponent high-entropy Cantor alloys. *Progress in Materials Science*, 2021, vol. 120, article number 100754. DOI: 10.1016/j.pmatsci.2020.100754.

5. Bertsch K.M., Nygren K.E., Wang S., Bei H., Nagao A. Hydrogen-enhanced compatibility constraint for intergranular failure in FCC FeNiCoCrMn high-entropy alloy. *Corrosion Science*, 2021, vol. 184, article number 109407. DOI: 10.1016/j.corsci.2021.109407.

6. Traversier M., Mestre-Rinn P., Peillon N., Rigal E., Boulnat X., Tancret F., Dhers J., Fraczkiewicz A. Nitrogen-induced hardening in an austenitic CrFeMnNi high-entropy alloy (HEA). *Materials Science and Engineering: A*, 2021, vol. 804, article number 140725. DOI: 10.1016/j.msea.2020.140725.

7. Klimova M., Shaysultanov D., Semenyuk A., Zherebtsov S., Salishchev G., Stepanov N. Effect of nitrogen on mechanical properties of CoCrFeMnNi high entropy alloy at room and cryogenic temperatures. *Journal of Alloys and Compounds*, 2020, vol. 849, article number 156633. DOI: 10.1016/j.jallcom.2020.156633.

8. Zhang Shidong, Liu Min, Luo Yun, Wang Lianbo, Wang Zemin, Wang Zhanyong, Li Fangjie, Shen Qin, Wang Xiaowei. Immunity of Al$_{0.25}$CoCrFeNi high-entropy alloy to hydrogen embrittlement. *Materials Science and Engineering: A*, 2021, vol. 821, article number 141590. DOI: 10.1016/j.msea.2021.141590.

9. Luo Hong, Li Zhiming, Lu Wenjun, Ponge D., Raabe D. Hydrogen embrittlement of an interstitial equimolar high-entropy alloy. *Corrosion Science*, 2018, vol. 136, pp. 403–408. DOI: 10.1016/j.corsci.2018.03.040.

10. Wu Z., Parish C.M., Bei H. Nano-twin mediated plasticity in carbon-containing FeNiCoCrMn high entropy alloys // Journal of Alloys and Compounds. 2015. Vol. 647. P. 815–822. DOI: 10.1016/j.jallcom.2015.05.224.

11. Wang Zhangwei, Baker I. Interstitial strengthening of a f.c.c. FeNiMnAlCr high entropy alloy. *Materials Letters*, 2016, vol. 180, pp. 153–156. DOI: 10.1016/j.matlet.2016.05.122.

12. Li Xinfeng, Yin Jing, Zhang Jin, Wang Yanfei, Song Xiaolong, Zhang Yong, Ren Xuechong. Hydrogen embrittlement and failure mechanisms of multi-principal element alloys: A review. *Journal of Materials Science & Technology*, 2022, vol. 122, pp. 20–32. DOI: 10.1016/j.jmst.2022.01.008.

13. Bhadeshia H.K.D.H. Prevention of hydrogen embrittlement in steels. *ISIJ international*, 2016, vol. 56, no. 1, pp. 24–36. DOI: 10.2355/isijinternational.ISIJINT-2015-430.

14. Lynch S. Hydrogen embrittlement phenomena and mechanisms. *Corrosion reviews*, 2012, vol. 30, no. 3-4, pp. 105–123. DOI: 10.1515/corrrev-2012-0502.

15. Panchenko M.Yu., Nifontov A.S., Astafurova E.G. Microstructural effect on hydrogen embrittlement of high nitrogen chromium-manganese steel. *Physical mesomechanics*, 2022, vol. 25, no. 5, pp. 453–465. DOI: 10.55652/1683-805X_2022_25_3_84.

16. Koyama M., Ichii K., Tsuzaki K., Grain refinement effect on hydrogen embrittlement resistance of an equiatomic CoCrFeMnNi high-entropy alloy. *International Journal of Hydrogen Energy*, 2019, vol. 44, no. 31, pp. 17163–17167. DOI: 10.1016/j.ijhydene.2019.04.280.

17. Fu Z.H., Yang B.J., Chen M., Gou G.Q., Chen H. Effect of recrystallization annealing treatment on the hydrogen embrittlement behavior of equimolar CoCrFeMnNi high entropy alloy. *International Journal of Hydrogen Energy*, 2021, vol. 46, no. 9, pp. 6970–6978. DOI: 10.1016/j.ijhydene.2020.11.154.

18. Bai Y., Momotani Y., Chen M.C., Shibata A., Tsuji N. Effect of grain refinement on hydrogen embrittlement behaviors of high-Mn TWIP steel. *Materials Science and Engineering: A*, 2016, vol. 651, pp. 935–944. DOI: 10.1016/j.msea.2015.11.017.

19. Park C., Kang N., Liu S. Effect of grain size on the resistance to hydrogen embrittlement of API 2W grade 60 steels using in situ slow-strain-rate testing. *Corrosion Science*, 2017, vol. 128, pp. 33–41. DOI: 10.1016/j.corsci.2017.08.032.

20. Fuchigami H., Minami H., Nagumo M. Effect of grain size on the susceptibility of martensitic steel to hydrogen-related failure. *Phil Mag Lett*, 2006, vol. 86, pp. 21–29.

21. Li J., Hallil A., Metsue A., Oudriss A., Bouhattate J., Feaugas X. Antagonist effects of grain boundaries between the trapping process and the fast diffusion path in nickel bicrystals. *Scientific Reports*, 2021, vol. 11, article number 15533. DOI: 10.1038/s41598-021-94107-6.

22. Owczarek E., Zakroczymski T. Hydrogen transport in a duplex stainless steel. *Acta Materialia*, 2000, vol. 48, no. 12, pp. 3059–3070. DOI: 10.1016/S1359-6454(00)00122-1.

23. Du Y.A., Ismer L., Rogal J., Hickel T., Neugebauer J., Drautz R. First-principles study on the interaction of H interstitials with grain boundaries in α- and γ-Fe. *Physical Review B*, 2011, vol. 84, article number 144121. DOI: 10.1103/PhysRevB.84.144121.

24. Oudriss A., Creus J., Bouhattate J., Savall C., Peraudeau B., Feaugas X. The diffusion and trapping of hydrogen along the grain boundaries in polycrystalline nickel. *Scripta Materialia*, 2012, vol. 66, no. 1, pp. 37–40. DOI: 10.1016/j.scriptamat.2011.09.036.

СПИСОК ЛИТЕРАТУРЫ

1. Feng Zheng, Li Xinfeng, Song Xiaolong, Gu Tang, Zhang Yong. Hydrogen Embrittlement of CoCrFeMnNi High-Entropy Alloy Compared with 304 and IN718 Alloys // Metals. 2022. Vol. 12. № 6. Article number 998. DOI: 10.3390/met12060998.

2. Zhao Yakai, Lee Dong-Hyun, Seok Moo-Young, Lee Jung-A, Phaniraj M.P., Suh Jin-Yoo, Ha Heon-Young, Kim Ju-Young, Ramamurty U., Jang Jae-il. Resistance of CoCrFeMnNi high-entropy alloy to gaseous hydrogen embrittlement // Scripta Materialia. 2017. Vol. 135. P. 54–58. DOI: 10.1016/j.scriptamat.2017.03.029.

3. Cantor B., Chang I.T.H., Knight P., Vincent A.J.B. Microstructural development in equiatomic multi-component alloys // Materials Science and Engineering: A. 2004. Vol. 375-377. P. 213–218. DOI: 10.1016/j.msea.2003.10.257.

4. Cantor B. Multicomponent high-entropy Cantor alloys // Progress in Materials Science. 2021. Vol. 120. Article number 100754. DOI: 10.1016/j.pmatsci.2020.100754.

5. Bertsch K.M., Nygren K.E., Wang S., Bei H., Nagao A. Hydrogen-enhanced compatibility constraint for intergranular failure in FCC FeNiCoCrMn high-entropy alloy // Corrosion Science. 2021. Vol. 184. Article number 109407. DOI: 10.1016/j.corsci.2021.109407.

6. Traversier M., Mestre-Rinn P., Peillon N., Rigal E., Boulnat X., Tancret F., Dhers J., Fraczkiewicz A. Nitrogen-induced hardening in an austenitic CrFeMnNi high-entropy alloy (HEA) // Materials Science and Engineering: A. 2021. Vol. 804. Article number 140725. DOI: 10.1016/j.msea.2020.140725.

7. Klimova M., Shaysultanov D., Semenyuk A., Zherebtsov S., Salishchev G., Stepanov N. Effect of nitrogen on mechanical properties of CoCrFeMnNi high entropy alloy at room and cryogenic temperatures // Journal of Alloys and Compounds. 2020. Vol. 849. Article number 156633. DOI: 10.1016/j.jallcom.2020.156633.

8. Zhang Shidong, Liu Min, Luo Yun, Wang Lianbo, Wang Zemin, Wang Zhanyong, Li Fangjie, Shen Qin, Wang Xiaowei. Immunity of $Al_{0.25}$CoCrFeNi high-entropy alloy to hydrogen embrittlement // Materials Science and Engineering: A. 2021. Vol. 821. Article number 141590. DOI: 10.1016/j.msea.2021.141590.

9. Luo Hong, Li Zhiming, Lu Wenjun, Ponge D., Raabe D. Hydrogen embrittlement of an interstitial equimolar high-entropy alloy // Corrosion Science. 2018. Vol. 136. P. 403–408. DOI: 10.1016/j.corsci.2018.03.040.

10. Wu Z., Parish C.M., Bei H. Nano-twin mediated plasticity in carbon-containing FeNiCoCrMn high entropy alloys // Journal of Alloys and Compounds. 2015. Vol. 647. P. 815–822. DOI: 10.1016/j.jallcom.2015.05.224.

11. Wang Zhangwei, Baker I. Interstitial strengthening of a f.c.c. FeNiMnAlCr high entropy alloy // Materials Letters. 2016. Vol. 180. P. 153–156. DOI: 10.1016/j.matlet.2016.05.122.

12. Li Xinfeng, Yin Jing, Zhang Jin, Wang Yanfei, Song Xiaolong, Zhang Yong, Ren Xuechong. Hydrogen embrittlement and failure mechanisms of multi-principal element alloys: A review // Journal of Materials Science & Technology. 2022. Vol. 122. P. 20–32. DOI: 10.1016/j.jmst.2022.01.008.

13. Bhadeshia H.K.D.H. Prevention of hydrogen embrittlement in steels // ISIJ international. 2016. Vol. 56. № 1. P. 24–36. DOI: 10.2355/isijinternational.ISIJINT-2015-430.

14. Lynch S. Hydrogen embrittlement phenomena and mechanisms // Corrosion reviews. 2012. Vol. 30. № 3-4. P. 105–123. DOI: 10.1515/corrrev-2012-0502.

15. Панченко М.Ю., Астафурова Е.Г., Нифонтов А.С. Влияние микроструктуры на особенности водородного охрупчивания высокоазотистой хромомарганцевой стали // Физическая мезомеханика. 2022. Т. 25. № 3. С. 84–97. DOI: 10.55652/1683-805X_2022_25_3_84.

16. Koyama M., Ichii K., Tsuzaki K., Grain refinement effect on hydrogen embrittlement resistance of an equiatomic CoCrFeMnNi high-entropy alloy // International Journal of Hydrogen Energy. 2019. Vol. 44. № 31. P. 17163–17167. DOI: 10.1016/j.ijhydene.2019.04.280.

17. Fu Z.H., Yang B.J., Chen M., Gou G.Q., Chen H. Effect of recrystallization annealing treatment on the hydrogen embrittlement behavior of equimolar CoCrFeMnNi high entropy alloy // International Journal of Hydrogen Energy. 2021. Vol. 46. № 9. P. 6970–6978. DOI: 10.1016/j.ijhydene.2020.11.154.

18. Bai Y., Momotani Y., Chen M.C., Shibata A., Tsuji N. Effect of grain refinement on hydrogen embrittlement behaviors of high-Mn TWIP steel // Materials Science and Engineering: A. 2016. Vol. 651. P. 935–944. DOI: 10.1016/j.msea.2015.11.017.

19. Park C., Kang N., Liu S. Effect of grain size on the resistance to hydrogen embrittlement of API 2W grade 60 steels using in situ slow-strain-rate testing // Corrosion Science. 2017. Vol. 128. P. 33–41. DOI: 10.1016/j.corsci.2017.08.032.

20. Fuchigami H., Minami H., Nagumo M. Effect of grain size on the susceptibility of martensitic steel to hydrogen-related failure // Philosophical Magazine Letters. 2006. Vol. 86. P. 21–29. DOI: 10.1080/09500830500482316.

21. Li J., Hallil A., Metsue A., Oudriss A., Bouhattate J., Feaugas X. Antagonist effects of grain boundaries between the trapping process and the fast diffusion path in nickel bicrystals // Scientific Reports. 2021. Vol. 11. Article number 15533. DOI: 10.1038/s41598-021-94107-6.

22. Owczarek E., Zakroczymski T. Hydrogen transport in a duplex stainless steel // Acta Materialia. 2000. Vol. 48. № 12. P. 3059–3070. DOI: 10.1016/S1359-6454(00)00122-1.

23. Du Y.A., Ismer L., Rogal J., Hickel T., Neugebauer J., Drautz R. First-principles study on the interaction of H interstitials with grain boundaries in α- and γ-Fe // Physical Review B. 2011. Vol. 84. Article number 144121. DOI: 10.1103/PhysRevB.84.144121.

24. Oudriss A., Creus J., Bouhattate J., Savall C., Peraudeau B., Feaugas X. The diffusion and trapping of hydrogen along the grain boundaries in polycrystalline nickel // Scripta Materialia. 2012. Vol. 66. № 1. P. 37–40. DOI: 10.1016/j.scriptamat.2011.09.036.

Влияние размера зерна на закономерности водородного охрупчивания многокомпонентного сплава (FeCrNiMnCo)₉₉N₁

© 2024

Гуртова Дарья Юрьевна[*,1], студент
Панченко Марина Юрьевна[2,3], младший научный сотрудник
лаборатории физики иерархических структур в металлах и сплавах
Мельников Евгений Васильевич[2,4], младший научный сотрудник
лаборатории физики иерархических структур в металлах и сплавах
Астапов Денис Олегович[1,5], студент
Астафурова Елена Геннадьевна[2,6], доктор физико-математических наук,
заведующий лабораторией физики иерархических структур в металлах и сплавах

[1]*Томский государственный университет, Томск (Россия)*
[2]*Институт физики прочности и материаловедения Сибирского отделения РАН, Томск (Россия)*

*E-mail: dasha_gurtova@mail.ru

[3]ORCID: https://orcid.org/0000-0003-0236-2227
[4]ORCID: https://orcid.org/0000-0001-8238-6055
[5]ORCID: https://orcid.org/0000-0002-1277-4180
[6]ORCID: https://orcid.org/0000-0002-1995-4205

Аннотация: Проблема водородного охрупчивания остается актуальной во многих сферах, поэтому повышенный интерес среди исследователей вызывает сплав FeCrNiMnCo (сплав Кантора) как один из наименее подверженных негативному воздействию водорода материалов. Тем не менее малоизученным остается вопрос о влиянии параметров микроструктуры на закономерности водородного охрупчивания сплава Кантора и многокомпонентных сплавов системы FeCrNiMnCo в целом. В работе изучено влияние размера зерна на склонность высокоэнтропийного сплава Кантора, легированного азотом, к водородной хрупкости. Для этого с помощью термомеханических обработок в сплаве (FeCrNiMnCo)₉₉N₁ были сформированы состояния с разным размером зерен (43±21, 120±57 и 221±97 мкм). Экспериментально установлено, что измельчение зерна приводит к увеличению прочностных свойств исследуемого сплава и способствует повышению устойчивости к эффектам водородной хрупкости: в образцах с наименьшим из представленных размером зерна водородно-индуцируемое снижение пластичности меньше, чем в образцах с наибольшим размером зерна. Уменьшение размера зерна вызывает также снижение длины хрупкой зоны, выявляемой на поверхностях разрушения образцов после растяжения. Это вызвано снижением диффузии водорода в процессе насыщения и уменьшением транспорта атомов водорода с подвижными дислокациями в процессе пластической деформации за счет уменьшения размера зерна.

Ключевые слова: водородное охрупчивание; многокомпонентные сплавы; высокоэнтропийные сплавы; сплав Кантора; (FeCrNiMnCo)₉₉N₁; водородная хрупкость; водородно-индуцируемая хрупкая зона; границы зерен; разрушение; механические свойства.